**TITLE:** **Temperature stability requirements at the interface between the ECCOSORB sky-load and its support in the LFI cryo-facility**

**DOC. TYPE:** Specification Document
**PROJECT REF.:** PL-LFI-PST-TN-059 **PAGE:** I of IV, 12
**ISSUE/REV.:** Issue 1.0 **DATE:** October, 2004

| | | |
|---|---|---|
| **Prepared by** | **L. Terenzi**<br>**G. Morgante**<br>**M. Lapolla**<br>**L. Valenziano**<br>**F. Cuttaia**<br>**A. Mennella**<br>**LFI System Team** | **Date:** October 10th, 2004<br>**Signature:** |
| **Agreed by** | **M. BERSANELLI**<br>**LFI Instrument Scientist**<br>**C. BUTLER**<br>**LFI Program Manager** | **Date:** October 10th, 2004<br>**Signature:** |
| **Approved by** | **N. MANDOLESI**<br>**LFI Principal Investigator** | **Date:** October 10th, 2004<br>**Signature:** |

# DISTRIBUTION LIST

| Recipient | Company / Institute | E-mail address | Sent |
|---|---|---|---|
| J. MARTI-CANALES | ESA – Noordwijk | Javier.Marti.Canales@esa.int | Yes |
| J. GROMKE | ESA – Noordwijk | | Yes |
| B. COLLAUDIN | ALCATEL – Cannes | bernard.collaudin@space.alcatel.fr | Yes |
| J.P. CHAMBELLAND | ALCATEL – Cannes | Jean-Philippe.Chambelland@space.alcatel.fr | Yes |
| | CSL | | |
| N. MANDOLESI | IASF/CNR – Bologna | reno@bo.iasf.cnr.it | Yes |
| C. BUTLER | IASF/CNR – Bologna | butler@bo.iasf.cnr.it | Yes |
| F. VILLA | IASF/CNR – Bologna | villa@bo.iasf.cnr.it | Yes |
| L. VALENZIANO | IASF/CNR – Bologna | valenziano@bo.iasf.cnr.it | Yes |
| G. MORGANTE | IASF/CNR – Bologna | morgante@bo.iasf.cnr.it | Yes |
| L. TERENZI | IASF/CNR – Bologna | terenzi@bo.iasf.cnr.it | Yes |
| F. CUTTAIA | IASF/CNR – Bologna | cuttaia@bo.iasf.cnr.it | Yes |
| M. SANDRI | IASF/CNR – Bologna | sandri@bo.iasf.cnr.it | Yes |
| C. BURIGANA | IASF/CNR – Bologna | buriana@bo.iasf.cnr.it | Yes |
| A. MENNELLA | IASF/CNR – Milano | daniele@mi.iasf.cnr.it | Yes |
| M. BERSANELLI | UNIMI – Milano | marco@mi.iasf.cnr.it | Yes |
| D. MAINO | UNIMI – Milano | davide.maino@mi.infn.it | Yes |
| F. PASIAN | OAT – Trieste | pasian@ts.astro.it | Yes |
| M. MARIS | OAT – Trieste | maris@ts.astro.it | Yes |
| E. ALIPPI | LABEN – Vimodrone | alippi.e@laben.it | Yes |
| G. CAFAGNA | LABEN – Vimodrone | cafagna.g@laben.it | Yes |
| M. BALASINI | LABEN – Vimodrone | | |
| M. LAPOLLA | LABEN – Vimodrone | | |
| M. MICCOLIS | LABEN – Vimodrone | miccolis.m@laben.it | Yes |
| M. BISERNI | LABEN – Vimodrone | biserni.m@laben.it | Yes |
| F. MONZANI | LABEN – Vimodrone | monzani.f@laben.it | Yes |
| R. SILVESTRI | LABEN – Vimodrone | silvestri.r@laben.it | Yes |
| L. PAGAN | LABEN – Vimodrone | pagan.l@laben.it | Yes |
| G. BALDAN | LABEN – Vimodrone | baldan.g@laben.it | Yes |
| P. LEUTENEGGER | LABEN – Vimodrone | leutenegger.p@laben.it | Yes |
| P. BASTIA | LABEN – Vimodrone | bastia.p@laben.it | Yes |
| L. BOSCHINI | LABEN – Vimodrone | boschini.l@laben.it | Yes |
| J. TUOVINEN | MILLILAB – Finland | jussi.tuovinen@vtt.fi | Yes |
| J. VARIS | MILLILAB – Finland | jussi.varis@vtt.fi | Yes |
| N. HUGHES | Ylinen – Finland | Nicholas.Hughes@elektrobit.com | Yes |
| R. DAVIS | JBO – UK | rjd@jb.man.ac.uk | Yes |
| A. WILKINSON | JBO – UK | aw@jb.man.ac.uk | Yes |
| N. RODDIS | JBO – UK | nr@jb.man.ac.uk | Yes |
| D. KETTLE | JBO – UK | dkettle@jb.man.ac.uk | Yes |

| | | | |
|---|---|---|---|
| E. ARTAL | Univ. of Cantabria – Santander | artal@dicom.unican.es | Yes |
| B. AJA | Univ. of Cantabria – Santander | beatriz@dicom.unican.es | Yes |
| R. HOYLAND | IAC – Tenerife | rjh@ll.iac.es | Yes |
| S. LEVIN | JPL – Pasadena | steve@beta.jpl.nasa.gov | Yes |
| M. SEIFFERT | JPL – Pasadena | michael.d.seiffert@jpl.nasa.gov | Yes |
| T. GAIER | JPL – Pasadena | todd.gaier@jpl.nasa.gov | Yes |
| M. PRINA | JPL – Pasadena | Mauro.Prina@jpl.nasa.gov | Yes |
| P. MEINHOLD | UCSB – Santa Barbara | peterm@cfi.ucsb.edu | Yes |
| A. SIMONETTO | IFP/CNR – Milano | simonetto@ifp.cnr.it | Yes |
| C. SOZZI | IFP/CNR – Milano | sozzi@ifp.cnr.it | Yes |
| J.-M. LAMARRE | IAS – Orsay | lamarre@ias.u-psud.fr | Yes |
| J.-J. FOURMOND | IAS – Orsay | fourmond@ias.u-psud.fr | Yes |
| G. GUYOT | IAS – Orsay | guyot@ias.u-psud.fr | Yes |
| LFI SPCC | IASF/CNR – Bologna | lfispcc@tesre.bo.cnr.it | Yes |

# CHANGE RECORD

| Issue | Date | Sheet | Description of Change | Release |
|---|---|---|---|---|
| Issue 0.1 | April '04 | All | First issue of document (DRAFT) | |
| Issue 1.0 | October04 | | General revision | 1.0 |
| | | | | |
| | | | | |
| | | | | |
| | | | | |
| | | | | |
| | | | | |
| | | | | |
| | | | | |
| | | | | |
| | | | | |
| | | | | |
| | | | | |
| | | | | |
| | | | | |
| | | | | |
| | | | | |
| | | | | |
| | | | | |

# 1. Abstract

During the testing phase of the QM and FM LFI instrument, the integrated radiometer chain assemblies (RCAs) will be tested in a dedicated cryo facility. The input signal will be provided by an eccosorb load placed in front of the LFI feed horns that simulates the sky signal; the thermal stability of this sky load needs to be of the same order of the stability that is expected in flight for the primary and secondary mirrors, in order not to introduce uncertainties in the test results that may be difficult to interpret. In this document we derive the thermal stability requirements at the interface between the ECCOSORB sky load and its support starting from the signal stability requirements and considering the current knowledge concerning thermal conduction properties of the ECCOSORB at 20 K.

# 2. References

## 2.1 Applicable documents

[AD1] Bersanelli, M., Seiffert, M., Hoyland, R. and Mennella, A.: "Planck-LFI scientific requirements", PL-LFI-PST-SP-011-2.0, October 2002

[AD2] Mennella, A., Villa, F. and Burigana, C.: "LFI optical interfaces", PL-LFI-PST-TN-034-1.0, May 2002

[AD3] LFI Instrument Cryo - GSE Facility Design Description Document, TN.CSL.LAB.03002

[AD4] P. Radaelli, LFI Cryo-Facility Specification, TL 18074 issue 2

[AD5] LFI Instrument Cryo - GSE Facility Cooling down time and thermal stability analysis, TN.CSL.LAB.04001

## 2.2 Reference documents

[RD1] Rondeaux, F., Bredy, P. Ad Rey, J.M. : "Thermal conductivity measurements of epoxy systems at low temperature", Proceedings of Cryogenic Engineering Conference, July 2001

[RD3] J. C. Mather et al, *Calibrator Design for the COBE Far-Infrared Absolute Spectrophotometer (FIRAS)*, ApJ, 512, 511, 1999

[RD2] F. Cuttaia, L.Terenzi, L. Valenziano, *Planck LFI 30/44 GHz Sky Load Implementation,* PL-LFI-PST-TN-051, 2004

[REF4] F. Cuttaia, '*Simulation of RF performance of Planck cold load*', PL-LFI-PST-RP-005, June 2003

# 3. Introduction

## 3.1 The input-signal stability requirements

The control of unwanted systematic effects of instrumental and astrophysical nature is one of the most critical issues in reaching the Planck-LFI scientific performances. These effects must be kept at the level of few □K/pixel in the final maps, according to a detailed budget discussed in detail in [AD1], where all the systematic effects have been split according to their source.

Fluctuations entering directly through the feed horn beams are particularly critical, because they are transferred directly to the detected radiometric output mixed with the relevant astrophysical signal. Furthermore, if the spurious fluctuation is synchronous with the spacecraft spin frequency (1 r.p.m.) then the systematic effect cannot be disentangled (apart from particular cases) from the "true" sky signal.

In the Planck satellite the emissive surfaces surrounding the instrument focal plane (i.e. the telescope mirrors, the baffle and the coldest V-groove) are sources of potential spurious signals coupling with the receiver horns. These signals are usually referred to as *internal straylight*. In Table 1 (taken from [AD1]) we report the breakdown of the requirements of systematic errors caused by internal straylight signals in three frequency regions, i.e.: (i) fast, random fluctuations (in this case the effect is a degradation of the instrument sensitivity, so the requirement is given in terms of percentage of 1-second radiometer sensitivity), (ii) spin-synchronous fluctuations and (iii) periodic, non spin-synchronous, fluctuations. In the latter two cases the requirement is given in terms of the maximum error per pixel in the final map caused by the systematic effect.

***Table 1 – Breakdown of requirements on systematic errors caused by internal straylight***

| Source | % of $^{TM}T_{1\text{-}sec}$ | Error from spin synch. signals (∝K) | Error from periodic signals (∝K) |
|---|---|---|---|
| **Telescope** | 2% | 0.5 | 0.55 |
| **Baffle** | 2% | 0.5 | 0.55 |
| **Spacecraft** | 2% | 0.5 | 0.55 |
| *SVM* | *1%* | *0.29* | *0.31* |
| *SVM Ring I/F* | *2%* | *0.29* | *0.31* |
| *Solar panels* | *1%* | *0.29* | *0.31* |
| **HFI** | 2% | 0.5 | 0.55 |
| ***Total*** | ***4%*** | ***1*** | ***1.1*** |

The requirements in the above table have been translated into requirements on the thermal stability of the emissive surfaces responsible for these systematic effects (see [AD2] for a detailed discussion). These requirements are reported in Table 2, and Table 3.

***Table 2 – Planck telescope thermal stability requirements***

| | 30 GHz | 44 GHz | 70 GHz |
|---|---|---|---|

| | | | |
|---|---|---|---|
| □$T_{random}$ (□K !s) | 310 | 370 | 490 |
| □$T_{ss}$ (□K) | | 33 | |
| □$T_{periodic}$ (mK) | | 10 | |

***Table 3 – Thermal stability requirements of the Baffle and of the coldest V-groove***

| | **Baffle** | **Coldest V-groove** |
|---|---|---|
| □$T_{random}$ (mK !s) | 5.34 | 508 |
| □$T_{ss}$ (mK) | 0.57 | 54.5 |
| □$T_{periodic}$ (K) | 0.2 | 19.5 |

Although the above requirements strictly apply to the in-flight Planck thermal environment, it is nevertheless important that a similar degree of stability is reproduced during the RCA and RAA ground testing during which the individual radiometers and the whole receiver array will be characterised and calibrated. In fact if the tests were conducted with a signal much more unstable compared to what is expected in flight, it could be difficult to interpret the radiometric data and disentangle the instabilities caused by the receiver themselves from the effects caused by the experimental setup.

The most critical item in the cryo-chamber in this respect is represented by the sky-load, an ECCOSORB black-body that is placed in front of the LFI feeds and provides the input signal to the radiometers. In this note we derive the thermal stability requirements at the interface between this sky load and its support, starting from the scientific requirements defined in Table 1. It is worth mentioning that fluctuations at the level of the sky load represent one of the many contributions to *internal straylight* signals in the cryo chamber, although they are likely to be the most relevant ones. Discussion concerning other effects (e.g. the effect of temperature fluctuations in the 70 K shroud) will be the object of forthcoming notes.

## 3.2 The LFI cryo chamber thermal design

The chamber is made of stainless steel, it has a vertical axis and the internal diameter is 2.3 m. It is built in 2 parts, a lower flat fixed one, being the bottom part, and an upper removable part, called the cover. This cover is a cylinder 1.9 m height with a flange welded at the bottom and a 'decimal' flange that closes the top. A viton gasket is sealing both parts. Details on facility design are available in [AD3].

LFI is positioned in the chamber horizontally with FPU and BEU fixed on insulating supports while the waveguide support structures are suspended to an aluminium frame by thin rods or wires [AD4]. A thermal tent, surrounding the instrument till V-groove #1, provides the radiative environment. The shrouds of this tent are made of 2 mm thick copper plates. They are black painted on their inner surface and covered by MLI on their outer face. As the chamber, the thermal tent is built in 2 parts: a flat shroud fixed on the thermal tent supports, being the bottom part, and an upper part, the cover, fixed on the bottom part. The total surface of the tent is about 8 $m^2$.

The thermal tent is cooled down by two 20K cold heads. Flexible copper straps will be used between cold heads and shrouds [AD5].

The sky load, the reference load and the FEU cold plate are linked to a third 20K cold head. Two gas gap heat switches are placed between the cold head and the loads (sky and reference) to adjust the thermal link. The FPU cold plate is connected directly to the cold head by thermal straps. These parts are fitted with two temperature sensors and two or more heaters for temperature control.

At the level of the V-grooves the thermal interface for the wave guides is provided by six straps (two for each V-Groove) thermally linked to the thermal tent. These interfaces are regulated independently, with separate temperature probes and heaters.

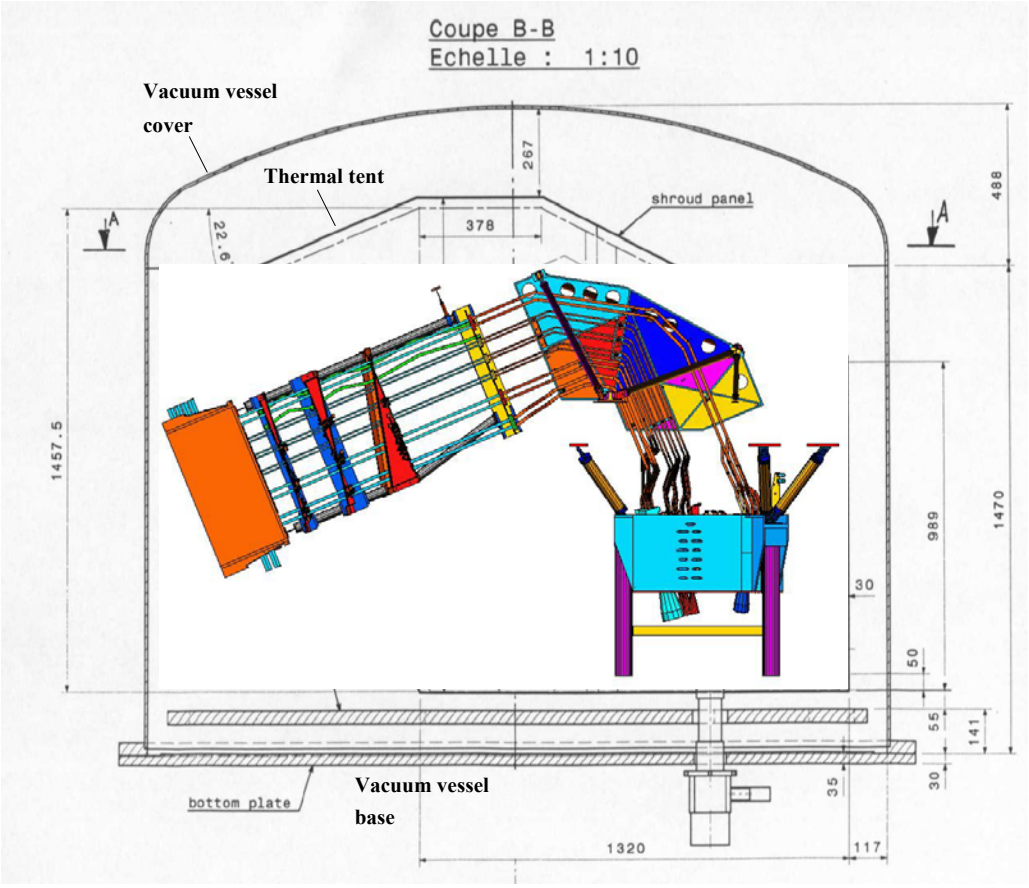


***Fig. 1 - the LFI instrument in the cryo-facility***

The BEU temperature will be regulated by a thermostatic bath that circulates liquid in copper pipes surrounding BEU interface plate. The temperature range for the BEU is 270–320 K, with a stability better than 0.1K.

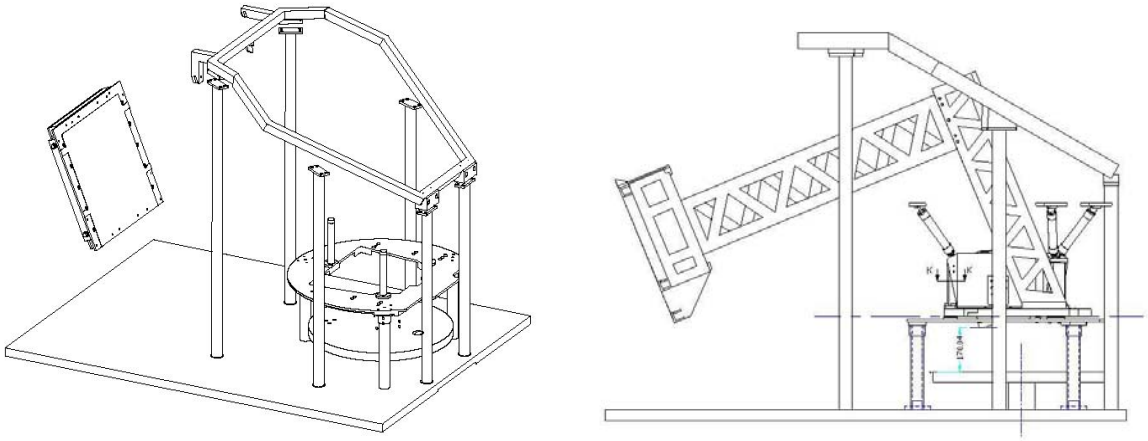

*Fig. 2 - The LFI insulating supports (left). Side view of LFI with cryo-MGSE and MGSE-2 (right). MGSE-2 is removed before tests.*

### 3.3 The sky load in the LFI cryo chamber

The sky load is a black body calibrator of polygonal shape made of ECCOSORB CR-110. It consists of a base layer 10mm thick covered by pyramids 5mm square base, 30 mm in height (see Fig. 3). The ECCOSORB calibrator is fixed (glued) to an aluminium plate 10 mm thick (TBC) of the same polygonal shape. This plate provides the mechanical and thermal interfaces for the calibrator

The calibrator is positioned in the facility horizontally, at a distance of 170 mm from the instrument feed-horns. It is fixed directly on the heat switch cylinders that provide cooling and mechanical support (see Fig. 4).

The gas-gap heat switch is interposed between the sky load and the cold head: when filled with gas it allows a fast cool-down of the sky load, otherwise it behaves like a thermal impedance allowing to warm up the sky load to 77 K while the FPU is at 20 K.

The aluminium plate is thermally controlled by means of temperature sensors and heaters connected to a PID controller.

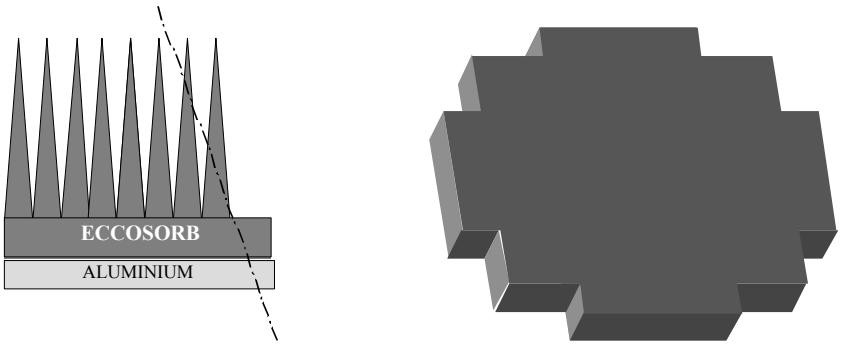

*Fig. 3 - Sky load cross section and polygonal layout.*

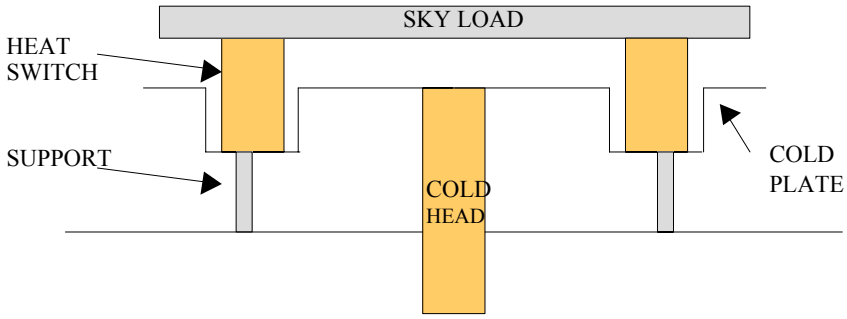


*Fig. 4 - The sky load mounted on the heat switch.*

# 4. Conversion from the radiometric signal stability to the physical temperature stability at the outer face of the sky load

In this section we discuss how the requirement on the radiometric input signal is converted into a requirement on the physical temperature stability of the sky load. To perform this computation we have used two separate analyses: a radio-frequency analysis to determine the radiometric input from the physical temperature distribution and a thermal analysis to evaluate the physical temperature distribution inside the load.

## 4.1 RF analysis

The RF analysis takes into account mainly two issues:

1. the antenna near field angular pattern evaluation at the three operational frequencies (30GHz, 44GHz, 70 GHz),

2. the evaluation of the load emissivity.

The first point is required since the power emitted by the load must be 'weighted' by the antenna pattern: the whole load can be considered formed of many discrete patches, each one, separately emitting, giving a contribution which depends only on the feed characteristics. The accuracy in the emissivity evaluation depends on the knowledge of the load electromagnetic characteristics (i.e. the electro magnetic parameters of its constituent material) at each frequency and on the ability of modelling the geometry.

For the near field pattern evaluation the code Grasp8 has been employed; to calculate the load emissivity a finite elements method analysis (using the code HFSS) has been performed [RD1].

The characterisation of the complete instrument (LFI) behaviour is reduced to the study of the single feeds (at 30GHz, 44GHz, 70GHz) facing the load.

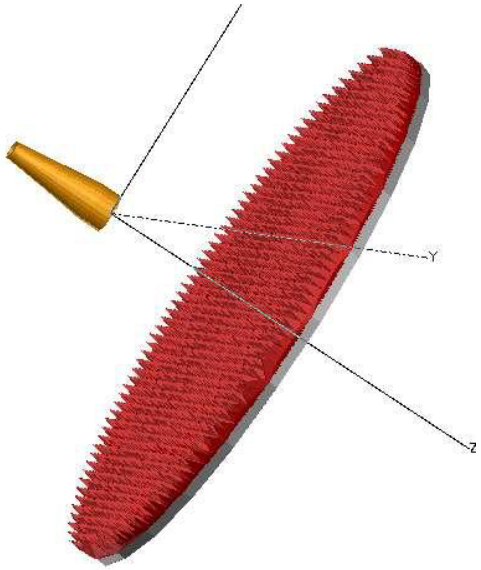


***Fig. 5 pictorial representation of a feed horn facing the sky load.***

The problem is analysed in transmission (from the feed to the load): the obtained result will be successively reverted (to evaluate the radiation emitted by the load and received by the feed) by applying the Reciprocity Theorem and the Kirchoff Law. A given power is radiated from the feed horn to the reference sky load that absorbs the most of it. Only a little part ($R_L$) of the initial power is back scattered towards the feed and another little power ($SPO_R$) is scattered towards the surrounding environment. The $R_L$ is mainly constituted of two components: one directly back-reflected at the impedance interface vacuum-absorber, and another back-reflected by the metal short placed behind the absorber (after the radiation having crossed the absorber section twice). A remaining part of the power emitted by the horn is not intercepted by the load and directly propagates in the surrounding. This contribution is named Direct Spillover ($SPO_D$) and can be estimated as the power emitted by the feed horn under the solid angle not filled by the load.
The total power can be written as:

$$P_{TOTAL} = SPO_D + SPO_R \cdot R_L + P_{ABS} \tag{1}$$

With:

$$SPO_D = \frac{\int_{180}^{180} P(\theta)\sin\theta\, d\theta}{\int_{0}^{180_{LOAD}} P(\theta)\sin\theta\, d\theta}$$

$$R_L = S_{11}^2 \tag{2}$$

$$SPO_R = \frac{\int_{0}^{180_{LOAD}} P(\theta)\sin\theta\, d\theta}{\int_{0}^{180} P(\theta)\sin\theta\, d\theta}$$

and the Total Reflectivity R can be written as:

$$R = SPO_R \cdot R_L - R_H \tag{3}$$

$$\int_{0}^{180_{LOAD}} P(\theta)\sin\theta\, d\theta$$

Where $R_H$ is the characteristic impedance at the feed aperture.

So, we can test the emitting properties of the load by radiating it with a radiation $P_{IN}$ and evaluating the absorption $P_{ABS} = P_{IN} - SPO_D - SPO_R \$ R_L$ by means of a measure of reflected power.

Then:

$$P_{EMITTED} = \int_{\Omega} P_{ABS}(\theta,\phi,T(\theta,\phi))\, d\Omega \qquad (4)$$

where $\varepsilon$ is the load emissivity; it depends on different factors: electromagnetic parameters (fixed for each frequency), material thickness (absorption increases with thickness, reflection keeps almost constant behind a certain characteristic thickness), incidence angle (changes the crossed thickness), geometry, surface machining (ruling on the reflectance and on the diffusivity: it strictly depends on the wavelength ).

For a perfect black body, at a certain frequency and temperature, by definition, is $\varepsilon_{ABS}(\theta,\phi,T) = 1$ .

## 4.2 Joining the RF to the thermal properties: the equivalent temperature

Once the angular *power pattern distribution* $P(\theta)$ of the feed and the intrinsic reflectivity $R$ at each frequency are known, we must relate them to the physical temperature, $T(\theta)$, to describe the environment seen by the feed in terms of a single parameter, which we define as normalised equivalent temperature.
Taking the origin of our reference system coincident with the centre of the feed aperture, as a first step we can reduce the problem to a two dimensional representation in the plane $[xz]$, where the $x$ axis lies on the aperture plane and the $z$ axis coincides with the feed horn axis.

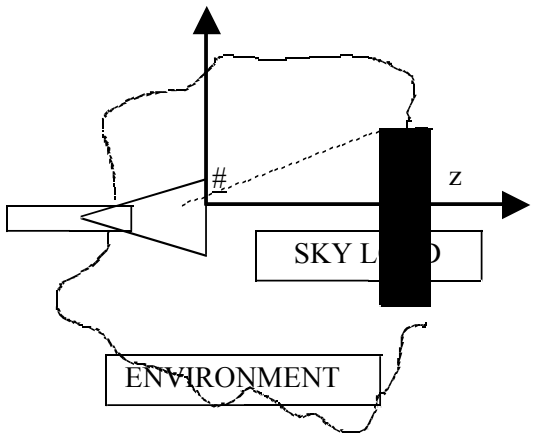


We define *effective emissivity pattern* $P_\varepsilon(\theta)$ the convolution product of the *power pattern distribution* with the angular emissivity pattern.

$$P_\varepsilon(\theta,\phi) = \int_{\Omega'} P_\varepsilon(\theta,\phi)\, P(\theta,\phi)\, d\Omega' \qquad (5)$$

In this frame, the *normalized equivalent temperature* (since the emissivity pattern is normalized to the total power emitted by the feed horn) can be defined as the convolution product of the *effective emissivity pattern* with the temperature angular distribution [RD2]. Both the quantities can be expressed in function of the angle θ between the z axis and the vector joining the origin with the middle point of the considered section.

So, the entire structure reduces to a discrete succession of elements, each one characterized by a constant (at a specific time) temperature, by its effective emissivity (depending on the emitting surface subtended by that angle) and the angle θ subtended.

The LOAD can be subdivided in annular regions of 1°; the environment, at this step, is considered as a box having homogeneous properties in terms of temperature and specific emissivity.

Two models can be studied in this combined method: stationary and transient.

### *4.2.1 Stationary model*

At first, we can evaluate the steady state temperature distribution, assuming the different stages fixed at their nominal temperatures, without any fluctuation. In this case, the convolution of thermal and RF parameters is only dependent by the angular position of the different regions and can be written as:

$$T_{norm} = \int_{\&} P(\#) T(\#) d\# \quad (6)$$

### *4.2.2 Transient model*

Also the transient case can be investigated. Following the same procedures used to analyse the steady state, we consider the temperature varying following a certain law, obtaining a time varying equivalent temperature:

$$T_{eq}(t) = \int_{\&} P(\#) T(\#, t) d\# \quad (7)$$

The integral can be replaced by a series over all the Sky Load sections, individuated by the angle #. Once the thermal environment is well defined, we can check with this method different contribution to radiometer signal instability.

## 5. The thermal transfer function of the ECCOSORB at 20 K

A first order study can be developed considering the beam response as null outside the load. If we model the cold load as a circular flange, with total volume equivalent to the real structure volume, we can reduce the emitting surface to the flange one and put some stability requirements upon it.

### 5.1 The thermal conduction properties of ECCOSORB at cryogenic temperatures

The only data available in literature of ECCOSORB CR110 thermal properties at cryogenic temperatures are reported in [RD3]. Furthermore these published results concern only a narrow temperature range around 4 K. The measured thermal conductivity is 0.08 W/m K, while specific heat is represented by the function $c_p = 0.6\ T^{2.05}$ J/Kg K. This experimental (power) law was used to extrapolate specific heat at 20 K for our purposes.

A set of simulations to evaluate the thermal damping of the sky-load was run with three different values of conductivity (see Sect. 5.2). In this analysis an equivalent ECCOSORB thickness of 20 mm was assigned to the load in order to effectively simulate the thermal mass of the whole complex pyramidal structure.

Thermal conductivity was further estimated by comparing the measured properties of similar materials in the same temperature range [RD1]. A quasi linear behaviour is the best fit to the conductivity data of epoxy resins, such as Stycast 2850 or Eccobond, usually considered very similar to the CR110 resin. The main

difference is the presence in ECCOSORB of small iron spheres, that might alter the validity of such evaluation in a way that should be carefully evaluated. The value suggested by such comparison for ECCOSORB thermal conductivity at 20 K is around 0.4 W/m K. For these reasons, among the three conductivity values used in the simulations (0.08 W/m K, 0.26 W/m K and 0.70 W/m K, see Fig.??), it was decided to choose 0.26 W/m K, the closer to the extrapolated value, as our upper limit to set the stability requirement specification.

## 5.2 Thermal simulations of the thermal transfer function

A simple model was developed to study the temperature fluctuations transfer function between the temperature controlled metallic interface plate and the ECCOSORB emitting surface facing the LFI horns.
To compute the evolution of the temperature of the free end (top) of the ECCOSORB plate, an electrical equivalent one-dimensional modelling has been used.

In this simplified model we consider a uniform ECCOSORB layer 20 mm thick. This thickness allows to simulate a volume equivalent to the entire pyramidal structure. The model does not take into account the geometry of the pyramid layer.

The total thickness of the ECCOSORB plate is divided into N elements. Each element is represented by a resistance and a capacity arranged as an RC network. All the elements are then connected in series to constitute a chain of RC networks.

In this way the transfer function can be obtained by calculating the response of the network at different frequencies.

The values for capacity and resistance to be used in the model can be calculated from the thermal properties of the material:

$$C = \int C_p S \, d*$$

$$R = \frac{1}{k} \frac{d*}{S}$$

$$d* = \frac{*}{N}$$

Where:

| | |
|---|---|
| % | is the ECCOSORB density |
| $k$ | is the thermal ECCOSORB conductivity |
| $Cp$ | is the ECCOSORB specific heat |
| * | is the ECCOSORB plate total thickness |
| $N$ | is the number of elements |
| $S$ | is the surface of the element cross section |

Since ECCOSORB data at 20 K are not available from the literature, the values have been extrapolated from existing data at 4 K and the cryogenic behaviour of known material. Three possible values of thermal conductivity have been considered: $k$ = 0.08; 0.26; 0.70 W/m-K

The first value is the same conductivity as at 4K which can be considered the lower limit . The second has been extrapolated considering materials that have characteristics similar to Eccosorb (epoxy). The highest value has been extrapolated considering materials that show a big increase in conductivity with temperature (i.e. stainless steel).

The value of specific heat used in our simulations, according to literature data described in the previous section is: $Cp$ = 240 J/Kg-K

The transfer function has been calculated using PSPICE circuit simulator; 15 elements were used. The circuit is shown in Fig. 6.

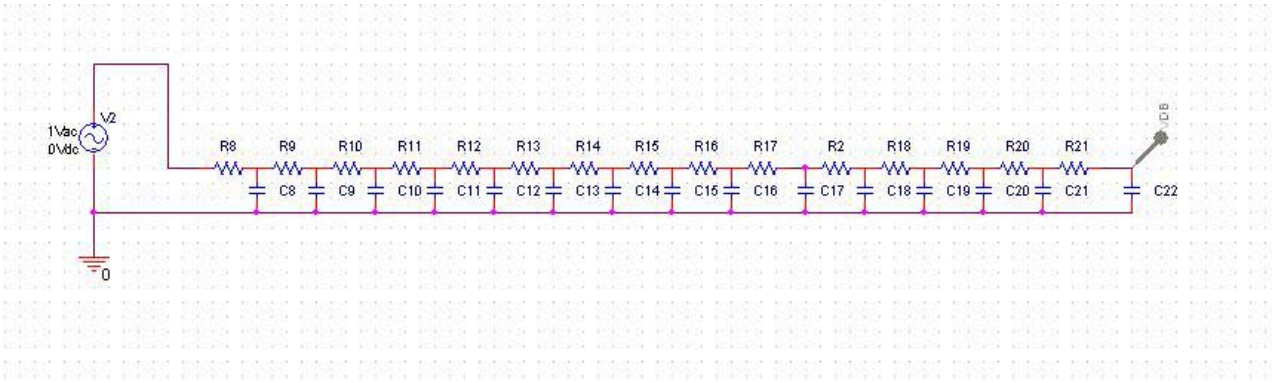


***Fig. 6 - PSPICE equivalent circuit***

The results of the simulation are presented in Fig. 7. The attenuation has been calculated on the amplitude data and are expressed in dB:

$$dB = 20 \log_{10} \frac{A_{out}}{A_{in}}$$

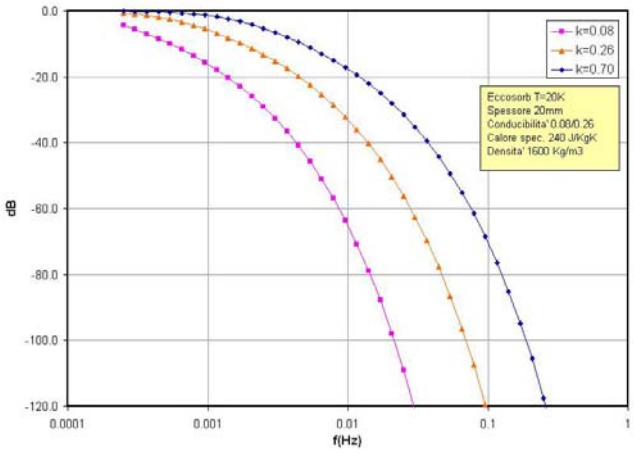


***Fig. 7 Fluctuation damping calculated with different conductivity values***

An equivalent thermal model was developed in Sinda in order to check the simulation results: Fig. 8 shows a comparison between the two models, both assuming a conductivity of 0.08 W/m K. Results are in good agreement, the small deviations at higher frequencies are due to the different number of nodes used.

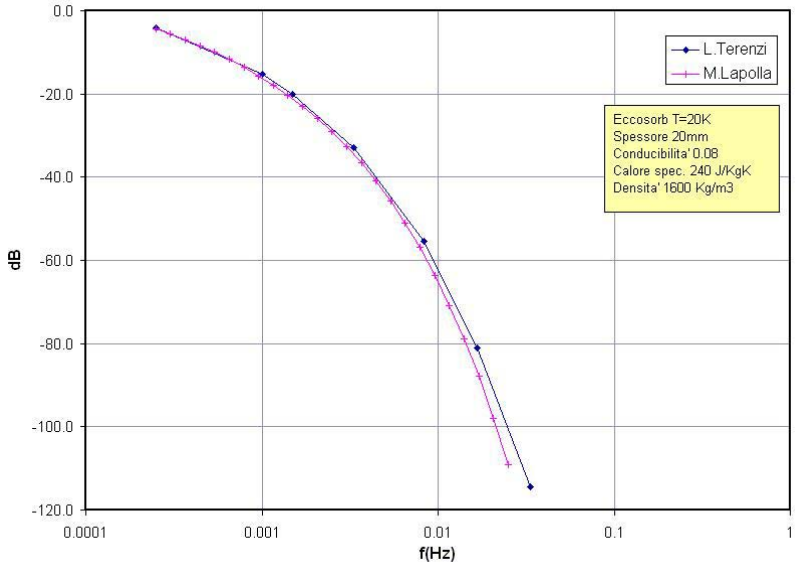


***Fig. 8 Comparison between the two models.***

## 6. The temperature stability requirement at the interface between the sky load and its support

The thermal control and temperature monitoring of the sky load are performed on the aluminium plate on which the Eccosorb calibrator is fixed. Therefore it is necessary that a temperature stability requirement is given at this interface.

To obtain this requirement we have started from the stability specification at the calibrator surface and then combined it with the behaviour of the Eccosorb layer presented in the previous paragraphs in order to estimate the corresponding stability near the temperature sensor.

### 6.1 Requirement at the Eccosorb surface.

Since thermal fluctuations at different frequencies have different impact on the radiometer performance, the temperature stability requirement has been defined as a power spectrum mask (see Fig. 9). The power spectrum density of the fluctuations at the calibrator surface must be kept within this mask.

The low frequency end is placed at 0.25 mHz (approximately 1 hour), a period of time which is compatible with the duration of one acquisition run. The deep notch centred at 0.016Hz corresponds to the spin synchronous frequency where the requirement is more stringent. In Table 4 the numerical values of the mask are presented along with the RMS values integrated over each segment of the mask.

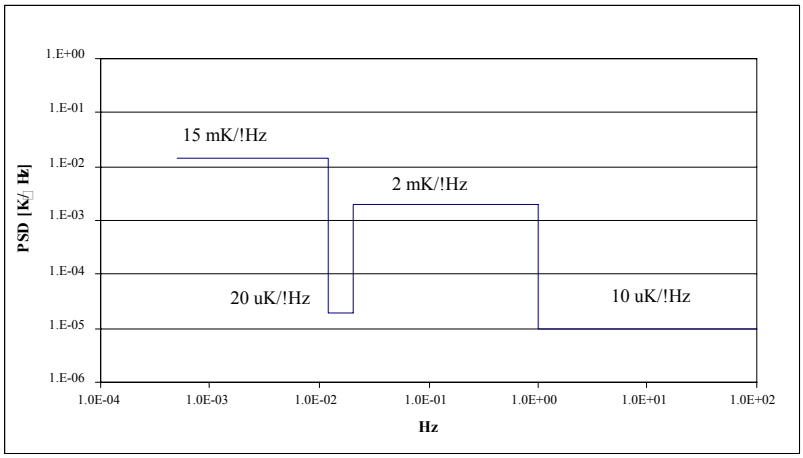


*Fig. 9 - Scientific requirements for the calibrator*

*Table 4 - Numerical values of the mask segments.*

| **Band** | **PSD**<br><br>**K/(Hz^0.5)** | **RMS integrated over the band** |
|---|---|---|
| 0.25mHz to 12mHz | $15 * 10^{-3}$ | 1.6mK |
| 12mHz to 20mHz | $20 * 10^{-6}$ | 1.8 µK |
| 20mHz to 1Hz | $2 * 10^{-3}$ | 2mK |

## 6.2 Requirement at the aluminium plate.

The requirement at the interface plate has been obtained applying the Eccosorb transfer function to the mask for the Eccosorb surface. As explained in Section 5.1 the curve with k = 0.26 has been chosen to be our best guess of the material property. The new mask is presented in Fig. 10 and Table 5.

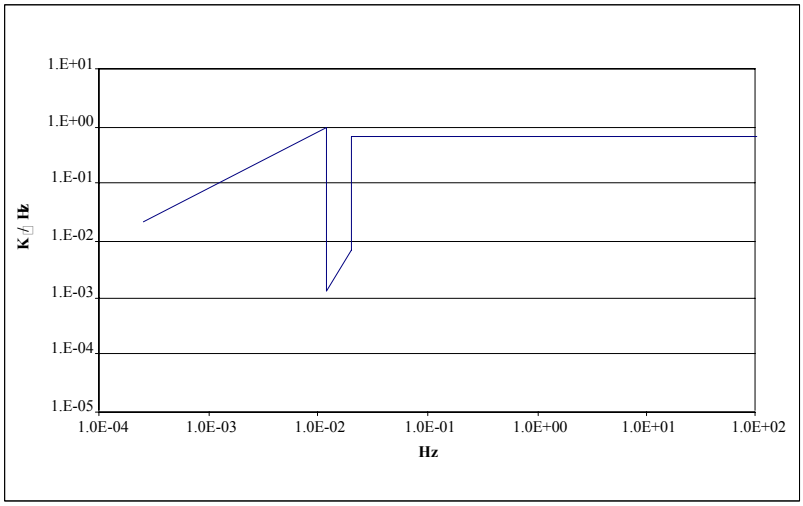


*Fig. 10 - Stability requirements at the aluminium plate.*

***Table 5 - Numerical values for the mask segments.***

| point | frequency [mHz] | PSD [mK/√Hz] |
|---|---|---|
| 1 | 0.25 | 20 |
| 2 | 12 | 940 |
| 3 | 12 | 1.3 |
| 4 | 20 | 6.5 |
| 5 | 20 | 650 |

## 7. Conclusions

In this document we have specified the thermal stability requirements of the sky load that will be used during the LFI QM and FM tests in the large cryo-facility in Laben. These requirements have been derived starting from the scientific requirements specified in [AD1] and then considering the thermal-electrical properties expected for the ECCOSORB load at 20 K.

A similar procedure can be applied to derive similar requirements for the sky load that will be used in the small cryo facility used for the RCA tests at 30 and 44 GHz. These will be the objective of a forthcoming specification document.

The effect of second-order instabilities induced by fluctuations in the radiative environment will be object of future analyses, and detailed requirements will be formulated in case significant effects will be highlighted.